Development of Formation Flying Sensors for External Occulters

Technology Development for Exoplanet Missions

PI: Webster Cash[1]
Anthony Harness[1], Ann Shipley[1], Steve Warwick[2]

November 29, 2015

Document #: 1514264

[1]University of Colorado Boulder
[2]Northrop Grumman Aerospace Systems

Approvals:

E-SIGNED by Webster Cash
on 2015-12-18 22:59:34 GMT

Webster Cash, Principal Investigator — Date
University of Colorado

E-SIGNED by Nick Siegler
on 2015-12-19 03:46:03 GMT

Nicholas Siegler, Technology Manager — Date
Exoplanet Exploration Program

E-SIGNED by Douglas Hudgins
on 2015-12-21 14:57:46 GMT

Douglas Hudgins, Program Scientist — Date
Exoplanet Exploration Program, NASA HQ

Table of Contents

1. Objective

This whitepaper details the development plan for and purpose of the Technology Development for Exoplanet Missions (TDEM) milestones to develop and demonstrate technologies critical to the formation flying of starshades. This study will investigate using long wavelength light diffracted around a starshade to provide accurate position information over large separations and advance the technology of a pupil imaging formation flying sensor. This will be the first investigation of starshades at wavelengths $\lambda > 1.5$ μm and will provide a critical datum for validation of optical models used to predict starshade performance.

2. Introduction

To find and characterize an Earth-like planet around a distant star requires a system capable of achieving high-contrast (10^{-10}) at small angles (0.1 arcseconds) to the host star. Starshades have been identified as a technology that can achieve the required starlight suppression at small inner working angles to make such discoveries (Cash, 2006).

The rapid decline in contrast as you move radially from the center of the starshade's shadow places a tight constraint on the lateral position of the starshade relative to the telescope-star line of sight. Maintaining alignment is imperative to achieving the science goals of an Earth finding mission. The New Worlds Observer (NWO) starshade architecture calls for a 60 m starshade flying at 80,000 km separation (Cash et al., 2009). This size starshade needs to hold lateral line of sight alignment to 1 m, requiring position knowledge of 10 cm. While the control requirements of formation flying at L2 may not be beyond current capabilities, the accuracy of position sensing at such large separations is unprecedented.

This study will aim to demonstrate the principles behind the technology needed to make these measurements. We will focus on a proposed sensor, the *Arago Sensor*, that uses long wavelength light diffracted around the starshade (a phenomenon known as the Spot of Arago) to map the wavefront distribution of light at the aperture of the science telescope and guide to the center of the starshade's shadow (Noecker, 2007).

2.1. Arago Sensor

The starshade's performance degrades steeply with increasing wavelength (suppression $\propto \lambda^{12}$). For a given separation, as the wavelength increases ($\lambda > 1$ μm), the size of the Fresnel half-zones increase and become comparable to the change across the apodization function, making the starshade appear as a circular disk to the incoming light. Light diffracted around the edge of the starshade reaches the optical axis in phase and constructively interferes to recover to its unblocked intensity, producing a phenomenon known as the **Spot of Arago**. Figure 1 shows the recovered intensity fraction as a function of wavelength for the NWO mission parameters (see Table 1), demonstrating the steep increase with wavelength. A unique property of the spot of Arago is that it is continuously formed along the optical axis, in other words, it has an infinite focal length. This means that as the starshade moves laterally, the spot is formed at the central axis of the starshade's new position and there

is a one-to-one mapping in the lateral position of the spot and that of the starshade. The spot forming at the telescope aperture is what allows us to detect sub-meter movements over megameters of separation. Imaging the pupil of the science telescope provides a map of the incident intensity at the aperture and the center of the spot of Arago yields the position of the starshade to centimeter accuracy (Noecker, 2010). This unique diffraction property makes a pupil plane instrument extremely advantageous over a focal plane instrument that would need to sense angular measurements of < 0.25 mas in order to detect positions accurate to the centimeter level.

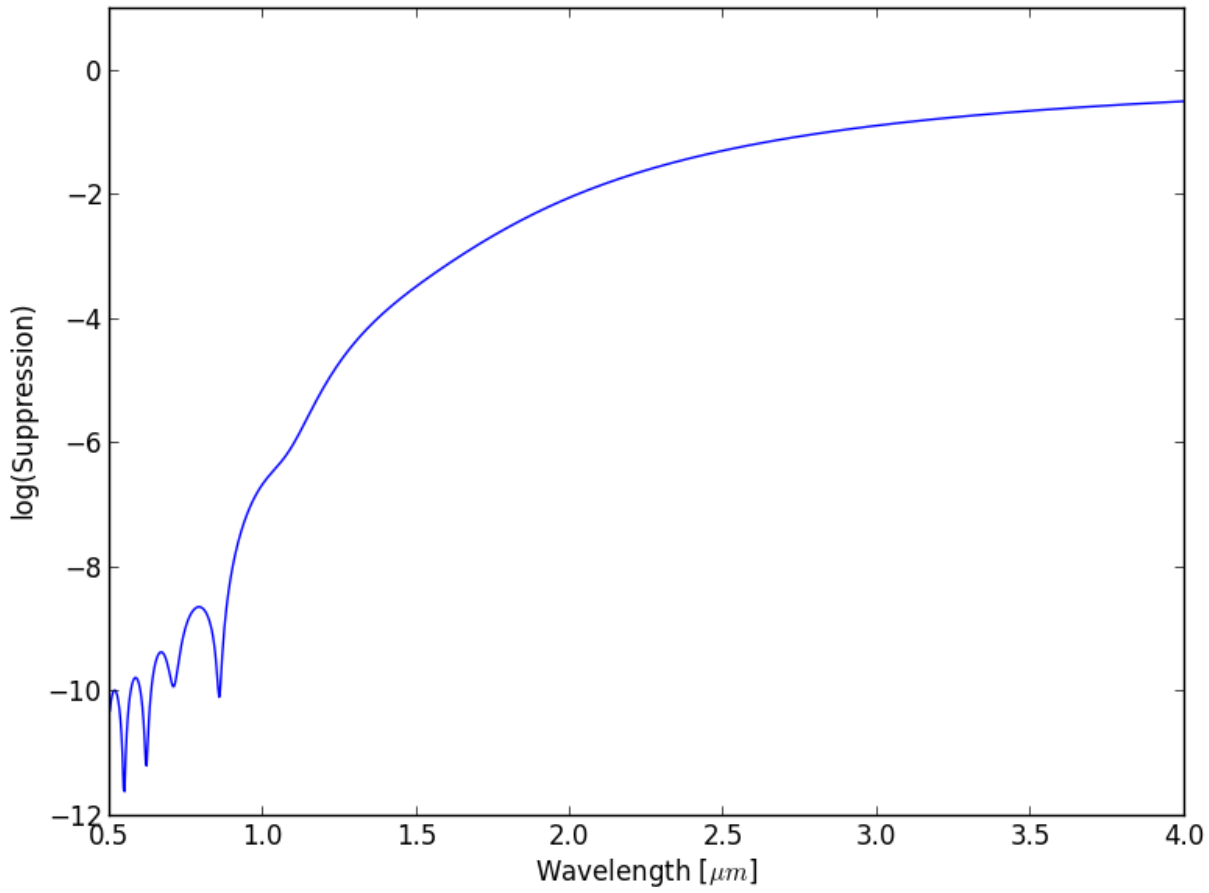

Figure 1: Simulation of the on-axis suppression as a function of wavelength for the NWO mission parameters given in Table 1.

At long wavelengths, the starshade can be approximated by a circular disk. The radius of this representative disk (r) can be approximated as the radius to the $1/e$ inflection point, $a+b$ (see Table 1). The resultant diffraction pattern can be determined by solving the Fresnel-Kirchoff diffraction equation for a circular obstruction. The intensity in the geometric shadow of the starshade $I(s)$, where s is the off-axis distance, can then be approximated by Equation 1 (Sommargren & Weaver, 1990), where V_n are the n^{th} order Lommel Functions of $u = \frac{kr^2}{F}$ and $v = \frac{krs}{F}$, k is the light wavenumber, F is the distance from the occulter to the observation

plane, and $J_n(x)$ is the n^{th} order Bessel function of the first kind.

$$I\left(s\right) = V_0^2\left(u,v\right) + V_1^2\left(u,v\right) \tag{1}$$

$$V_n\left(u,v\right) = \sum_{m=0}^{\infty} \left(-1\right)^m \left(\frac{v}{u}\right)^{n+2m} J_{n+2m}\left(v\right) \tag{2}$$

for $v << u$, we ignore the higher-order terms in Equation 2 and approximate the intensity

$$I(s) \approx J_0^2\left(v\right) \tag{3}$$

The half-width of the central peak of the spot of Arago can be approximated as the location of the first zero of J_0 and is given by Equation 4.

$$r_{SoA} \approx 0.38\frac{\lambda F_{eff}}{r} \tag{4}$$

Note that in Equation 4 we are using the effective separation (F_{eff}), due to the diverging light source. If F_1 is the distance from the source to the starshade, and F_2 is the distance from the starshade to the telescope, then F_{eff} is given by Equation 5. For our setup, $F_1 = F_2$ making $F_{eff} = \frac{1}{2}F_2$. Figure 2 shows the wavelength dependence of the shape of the diffraction pattern, most importantly the width of the central spot. At $\lambda = 2$ μm, the spot of Arago fills nearly the entire NWO aperture ($D = 4$ m).

$$F_{eff} = \frac{F_1 F_2}{F_1 + F_2} \tag{5}$$

As the spot of Arago is continuously formed along the optical axis of the starshade, there is a one-to-one mapping of the center of the spot of Arago incident on the aperture and the center of the starshade relative to the line of sight between telescope and star. This means that finding the center of the spot of Arago within the aperture will directly yield the lateral offset of the starshade, so the accuracy in the position knowledge is limited to how well we can find the true center of the spot of Arago. There are a number of complications that prevent a simple centroiding algorithm from being the best option:

- On-axis telescopes such as WFIRST have a complex, non-symmetric pupil which can bias the centroiding algorithm.
- As the spot moves towards the edge of the aperture in one direction, the centroid becomes biased towards the opposite direction as there is no flux contribution from beyond the edge of the aperture.
- If the spot center has moved off the edge of the aperture, centroiding will not find the center.

To get a more accurate position of the spot center, we can fit a model of the diffraction pattern to the image and solve for the center of the spot. Luckily, as we have shown earlier, the normally complex diffraction pattern from the starshade is much simpler at longer wavelengths and can be approximated by Equation 3. This allows for an efficient method to accurately solve for the starshade's position, even when the spot is off the aperture. Figure 3 shows a simulation of the pupil image of a off-center starshade, along with the model used to fit for the center of the spot in the pupil. In this study, we will investigate tradeoffs in position determination via model fitting versus a simple centroiding algorithm.

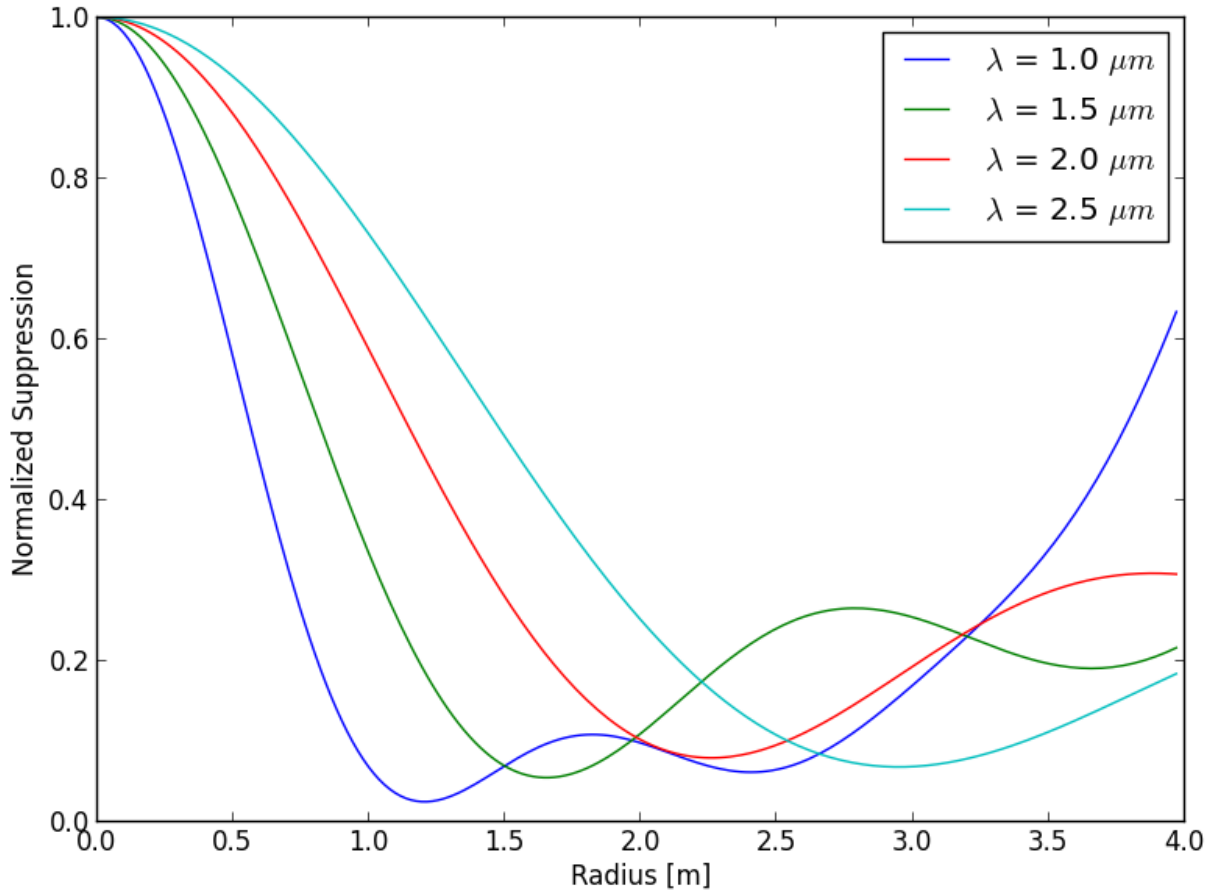

Figure 2: Simulation of the normalized suppression vs. radius and as a function of wavelength for the NWO mission parameters given in Table 1. This diagram demonstrates the affect wavelength has on the shape of the spot.

3. Milestone Definition

The major milestones to be completed in this study will advance the technology of a pupil imaging formation flying sensor for starshades and provide insight into the future design of such an instrument. The milestones we have chosen will demonstrate the starshade's performance degrades at long wavelengths as predicted by theory and that this degradation provides a useful guiding signal at adequate signal-to-noise. They will also demonstrate that

the spot of Arago provides a direct proxy of the starshade's position at large separations, can provide higher precision position information than obtainable with angular measurements in the focal plane, and that this signal can guide a telescope to the center of the shadow.

Two major milestones are defined as:

1. Demonstrate recovery of long wavelength ($\lambda > 1.5$ μm) light diffracted around starshade. Demonstrate agreement between starshade performance at these wavelengths and model predictions.

2. Demonstrate ability to use diffracted light to provide accurate measurements of the starshade's position while in its shadow.

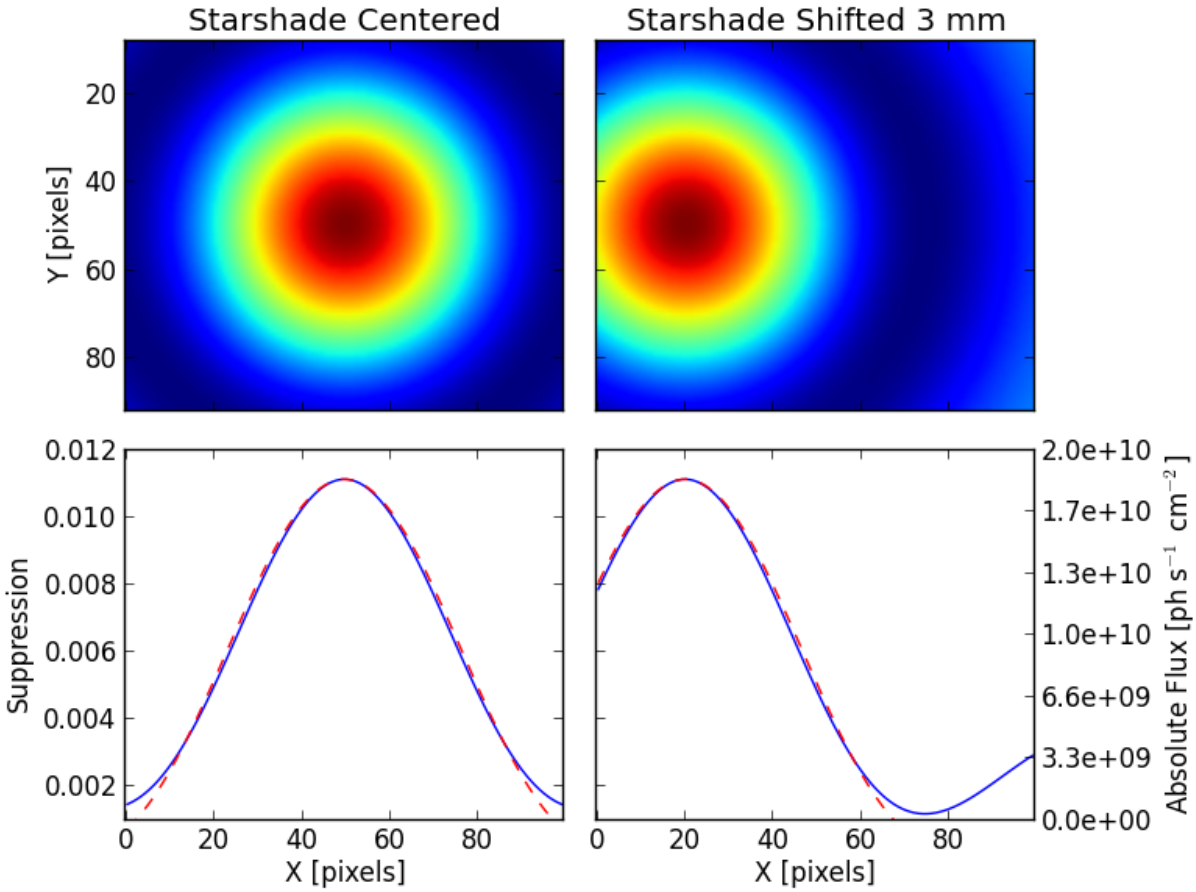

Figure 3: The **top** panel shows simulated pupil images using TDEM13 parameters of Table 1. In the **bottom** panel, the **blue** line is a cross-section of the image and the **red** dashed line is a model fit to the image using Equation 3. The **left** panel is when the starshade is centered on the aperture, the **right** panel is after the starshade has been shifted by 3 mm.

4. Experiment Description

For Milestone 1, the layout and test procedure of our experiment follow that of Glassman et al. (2014), except we will be observing at longer wavelengths and taking pupil plane, instead of focal plane, images. At one end of the setup will be a telescope with a NIR camera imaging the pupil plane (see Figure 4). We will use a commercial 6 inch telescope with various masks to stop down the size of our aperture. 2 kilometers away will be a bright artificial light source ($\lambda > 1$ μm). Halfway between will be a starshade on a translation stage. The prescription for the shape of the starshade is given by the hyper-Gaussian analytical solution presented in Cash (2006) and summarized in Table 2. In order to work with a starshade of a practical size, we will be using a 12 cm diameter (to the inflection point) starshade etched out of steel in a chemical bath. Starshades of this size have previously been demonstrated to provide sufficiently high-contrast (Glassman et al., 2014; Novicki et al., 2016). The physical parameters of the experiment are shown in Table 1 and compared to those of the proposed NWO mission (Cash et al., 2009) and the work of Glassman et al. (2014). Note that our experiment is conducted at flight-like Fresnel numbers.

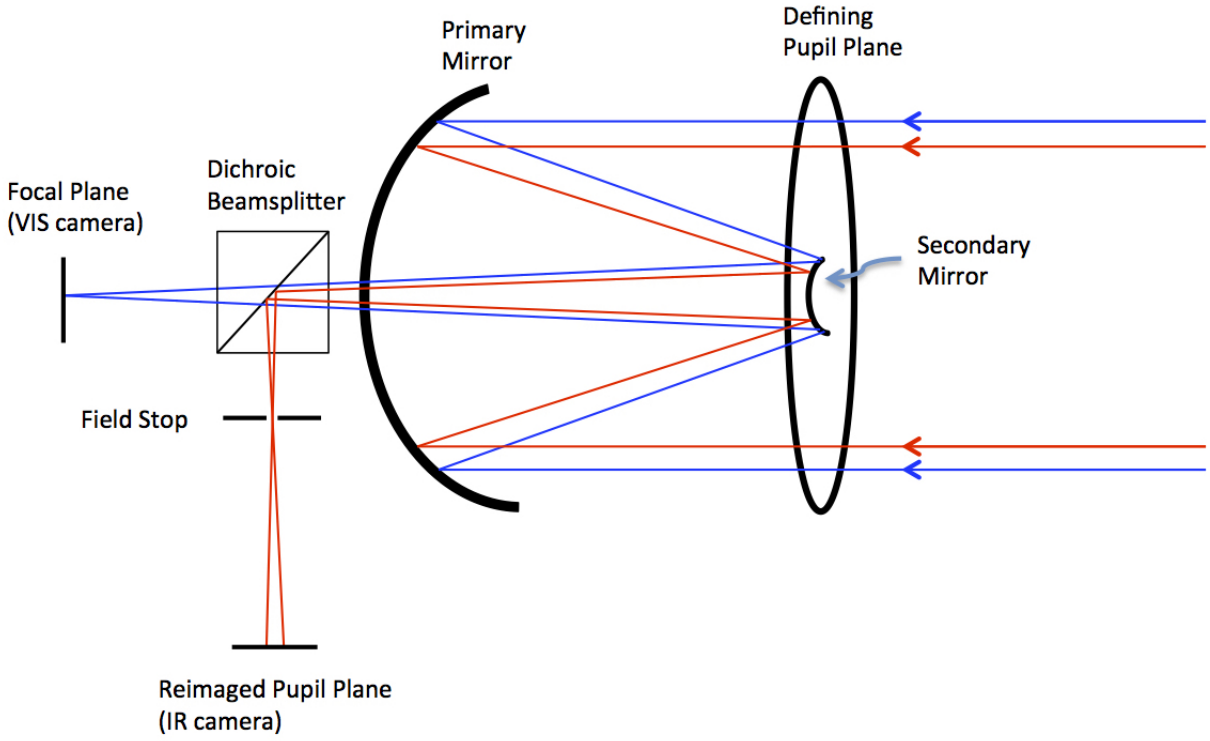

Figure 4: Schematic of optical layout with IR camera imaging the aperture (defining pupil) and visible light camera imaging the focal plane.

Mission/Mode	λ	$\mathbf{F}_{eff}$	$\mathbf{r}_{SS}$	N	$\mathbf{R}_{tel}$	$\mathbf{r}_{SoA}$
NWO Guiding	2 μm	80 Mm	25 m	3.9	2 m	2.5 m
TDEM13 Guiding	2 μm	500 m	6 cm	3.6	1 cm	6 mm
NWO Science	0.5 μm	80 Mm	25 m	15	2 m	-
TDEM13 Science	0.5 μm	500 m	6 cm	14	1 cm	-
NG TDEM Science	0.5 μm	500 m	24 cm	230	2 cm	-

Table 1: Physical parameters for a number of missions (full-scale NWO mission (Cash et al., 2009), this TDEM's work in the desert, and NGAS' previous TDEM work (Glassman et al., 2014)) and observing modes (guiding or science). λ is the wavelength of the observation, F_{eff} is the effective separation between starshade and telescope, $r = a + b$ is the radius of the starshade to its inflection point, N is the Fresnel number, R_{tel} is the aperture radius, and r_{SoA} is the radius of the spot of Arago at 2 μm. Note that this test is at a flight-like Fresnel number.

Variable	Parameter	Value
a	Offset radius of hyper-Gaussian	3 cm
b	$1/e$ radius of hyper-Gaussian	3 cm
n	Order of hyper-Gaussian	6
P	Number of petals	16

Table 2: Hyper-Gaussian starshade parameters used in this experiment. See Cash (2011) for a more detailed description of the hyper-Gaussian shape.

4.1. Optical System Description + Signal-to-Noise Calculations

The optical system is shown schematically in Figure 4, in which we use the secondary mirror of a 15 cm diameter Cassegrain telescope to reimage the defining pupil that is the aperture. A dichroic beamsplitter separates the light into infrared light reimaging the pupil plane and visible light imaging the focal plane. We will scale the pupil imaging camera so that 100 pixels cover a 2 cm diameter of the aperture (Noecker, 2010). We can alleviate the constraint on wandering of the spot due to the atmosphere, by allowing the field of view of the pupil imaging camera to extend the full aperture and creating 2 cm subapertures (spanned by 100 pixels) in software.

We baseline the artificial light source to output 1W optical power, which is focused to a 2.5° beam with a 85 mm camera lens, providing $\sim 10^{12}$ photons/s/cm^2 incident on our aperture. Assuming each pixel covers 200 μm of the aperture, a detector with 80% QE, and a recovered spot intensity of 1%, we expect $\sim 5 \times 10^6$ photons/s/pixel. We assume a detector readout noise of 60 e$^-$ and neglect any contribution from dust scattering to estimate a S/N of 100 with 2 ms integration (reading the camera at 300 fps). The brightness of the source and the level of recovered flux in the spot allow for short exposure times to help alleviate atmospheric effects. Figure 5 shows the estimated flux at the pupil as a function of wavelength. The flux (and S/N) drops dramatically with decreasing wavelength and the images will be dominated by longer wavelength light.

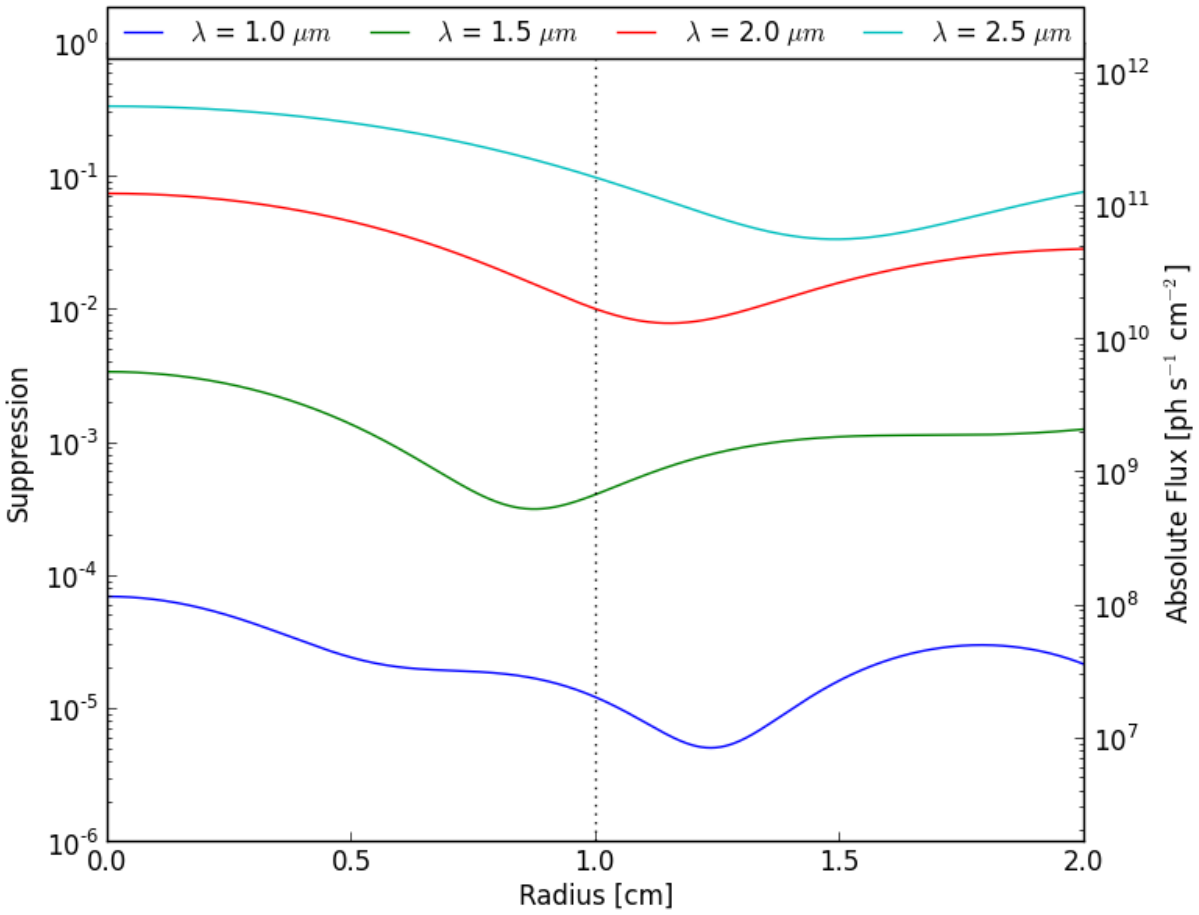

Figure 5: Simulated flux vs radius for different wavelengths using TDEM13 parameters in Table 1. The **left** axis is shown in units of suppression, the **right** axis is shown in absolute flux units [ph s^{-1} cm^{-2}]. The flux falls off dramatically at short wavelengths.

4.2. Dry Lake Bed Test Facility

We will complete our milestones performing all experiments on dry lake beds in open air. Dry lake beds are some of the flattest places on Earth and allow for the three-way alignment of a telescope, starshade, and artificial light source over kilometers of separation. We will utilize the dry lake bed test facility established with previous TDEM work led by the Northrop Grumman starshade team (Glassman et al., 2014), which has been proven to be an efficient way to test $1/100^{th}$-scale starshades. The latest results from those tests (Warwick et al., 2014; Glassman et al., 2015) show that the air beams are stable enough to perform high contrast imaging with starshades. In particular, it was shown that the fast twinkle of the atmosphere does not affect the light suppressing performance of the starshades. It was also shown there are longer timescale (i.e., minutes) drifts due to refraction in the atmosphere.

Extending to longer wavelengths will result in atmospheric effects much less problematic than for Glassman et al. (2015). The size of the atmospheric seeing disk, a characteristic length

scale at which atmospheric turbulence starts to significantly affect propagating wavefronts, increases as $\lambda^{6/5}$ (Fried, 1966). On a decently stable observing night, Glassman et al. (2015) saw an average of 8 arcseconds seeing, which gives a seeing disk size of $r_0 \sim 1.4$ cm at $\lambda = 0.55$ μm. At $\lambda = 2$ μm, this seeing disk size grows to $r_0 \sim 8$ cm and is larger than our aperture, meaning turbulence will not have a significant effect. Charnotskii (2011) found that the average Strehl number of the spot of Arago propagating through a turbulent medium is less susceptible to turbulence strength than that of conventional imaging. Time variations in atmospheric properties will lead to changes in transmission, but if we take our unblocked calibration images close in time to the blocked images, we can sample the same atmosphere and these effects will be mitigated. The increase in seeing disk size at longer wavelengths and imaging the spot of Arago in the pupil instead of conventional imaging lead us to believe atmospheric effects will not limit the success of the experiment. Figure 6 shows an image of the spot of Arago formed by the star Vega and demonstrates the spot of Arago can be formed in the atmosphere over a large separation. This setup consisted of a camera positioned 1 km behind a 8 cm circular disk as the star disappeared behind the disk and reemerged as the spot of Arago. While we are relying on previous experience to estimate the atmosphere will not prevent the milestones from being reached, we will use off-axis lights to monitor the atmosphere during observations and use those data to include atmospheric effects in our models.

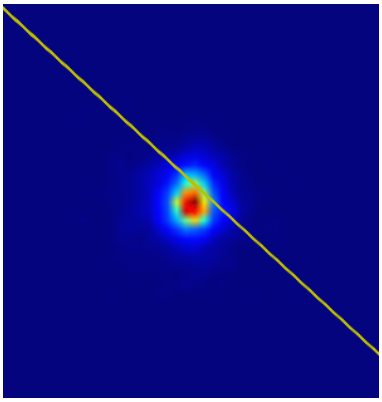

Figure 6: DSLR image of the spot of Arago produced by the star Vega, formed behind a 8 cm circular disk at a separation of 1 km.

An additional atmospheric effect that needs to be considered is the slow image wander due to changes in atmospheric refraction. As the desert floor cools after the sun sets, the thermal structure of the air directly above the ground changes and results in a wandering image of the main source. Glassman et al. (2015) saw a maximum apparent movement of the light source at the starshade's distance of 2 cm/s. Experience in previous desert tests have taught us at which time of night this effect is worse and that we should not bother observing during the worst conditions. This will shorten the amount of observing time available during each trip, but there will be periods of stable air in which we can observe unhindered. Taking shorter exposures (a luxury we are allowed when not trying to reach 10^{-9} contrast) will allow us to throw out bad images and combine the good ones to increase signal-to-noise. Again, observing at longer wavelengths will lessen this effect (Fried, 1966).

A limiting factor to the achievable contrast of Glassman et al. (2014) was forward scattering of the main source off dust in the atmosphere. The forward scattering created a smooth background at the 10^{-8} contrast level, well below our expected noise floor and therefore will not be a contributing factor to our results.

4.3. Optical Model Validation

The size scales of the space-based starshade mission make it impossible to fully test the starshade as a system on the ground. This forces us to rely on optical models, invoking scalar diffraction theory, to predict performance. Scalar diffraction theory tells us that if we preserve the Fresnel number (Equation 6), we maintain similarity and probe the same physics. This allows us to validate our models with a smaller system and use those results to predict performance on the large scale. Optical model validation was a major milestone in Glassman et al. (2014) and this TDEM will extend that work to an unexplored wavelength regime. We will measure the intensity distribution across the aperture for wavelengths > 1.5 μm, with the starshade at different lateral displacements. The results of each configuration will be compared against state of the art diffraction codes (Cash, 2011).

$$N = \frac{r^2}{\lambda F_{eff}} \tag{6}$$

An additional test that will be done if time allows, is to investigate the effect that tilting the starshade out of plane has on the formation of the spot of Arago. Glassman et al. (2014) has shown that tilting the starshade (up to 30°) has little effect on the light suppression performance of the starshade and we would like to verify that it will not have a strong effect on the guiding signal. Figure 7 shows a simulation of the pupil image for a starshade tilted by 20°. Tilting the starshade foreshortens one dimension of the starshade and as long as that smaller dimension does not enter an adjacent Fresnel half-zone (allowing 30° of tilt with our setup at $\lambda = 2$ μm), then the spot of Arago is still formed, but with a skewed PSF.

These tests, and the completion of Milestone 1, will help to validate these diffraction models in a parameter space not previously investigated and will help to define the robustness of the formation of the spot of Arago.

4.4. Starshade Positioning Tests

Milestone 2 will demonstrate the spot of Arago can be used to provide accurate position of the telescope in the starshade's shadow. This will be demonstrated through a number of positioning tests. The starshade will be mounted on a stage and stepped in precise movements across the field of view of the telescope, while images are taken at each step. The relative movement detected in the image will then be compared to the known movement of the starshade. In addition to the fast atmospheric twinkle ('seeing'), there will be a slow relative drift in the apparent position of the target source due to refraction in the atmosphere caused by temperature gradients above the desert floor. Experience in Glassman et al. (2014) has shown us that this effect is slow compared to our exposure time, and the effects can be mitigated by stacking multiple images. An off-axis light source set at the same height as the primary source will allow us to probe what the atmosphere is doing. In addition to detecting relative motion of the starshade, we would like to verify that we can use the spot of Arago to guide us to the center of the starshade. This will be done with human-in-the-loop visual feedback manually positioning the starshade to center over the telescope. We can verify we

are in the center of the shadow by imaging a symmetric distribution of visible light diffracted at the base of the petals.

4.5. Additional Tests

The following is a list of "nice to haves" i.e., tests that would be nice to complete should there be time in the schedule.

1. Vary aperture size to investigate effect of resolution on guiding signal and match flight-like resolution.
2. Obtain photometric measurements at narrow wavelength bands to reproduce Figure 1 and compare to models.
3. Investigate effect of tilting the starshade out of plane on the formation of the spot of Arago.
4. Investigate the effect an obscuring secondary mirror has on determining the location of the spot in the aperture.

4.6. Differences Between Laboratory Demonstrations and Flight

The starshades used in this experiment are $\sim 1/420^{th}$ the size of that in the NWO mission and we use an artificial, diverging light source instead of collimated starlight. The diverging beam acts to decrease the effective separation between starshade and telescope by half. The diverging beam also changes the 1-1 relation between the movements of the starshade and spot of Arago to a 1-2 relation, respectively. Table 1 summarizes these parameters and shows that we have scaled the experiment to be at a flight-like Fresnel number. This means the same optical models used to predict the performance of (and to be verified by) the small-scale tests can be used to predict the performance of the flight-like starshade.

The outdoor "laboratory" is a different environment than expected on orbit (in some senses less forgiving), but as demonstrated in Glassman et al. (2015), it should not affect the validity of our experiments. As mentioned in Section 4.2, the atmosphere will have a varying effect on light transmission, but will be accounted for with unblocked calibration images. The scattering of dust in the atmosphere should be a negligible background, and can easily be subtracted if present at higher levels than predicted.

5. Data Measurement & Analysis

The data product for each test will be pupil images recorded with a NIR detector, in the shadow of the starshade. The experimental methods for obtaining these data for the different milestones are explained in Section 4.

The analysis for Milestone 1 will be a comparison of the images to those generated by the numerical models. Comparison to the numerical models for will be done in units of *suppression*, in which the images are normalized by those of the unblocked source. The blocked and

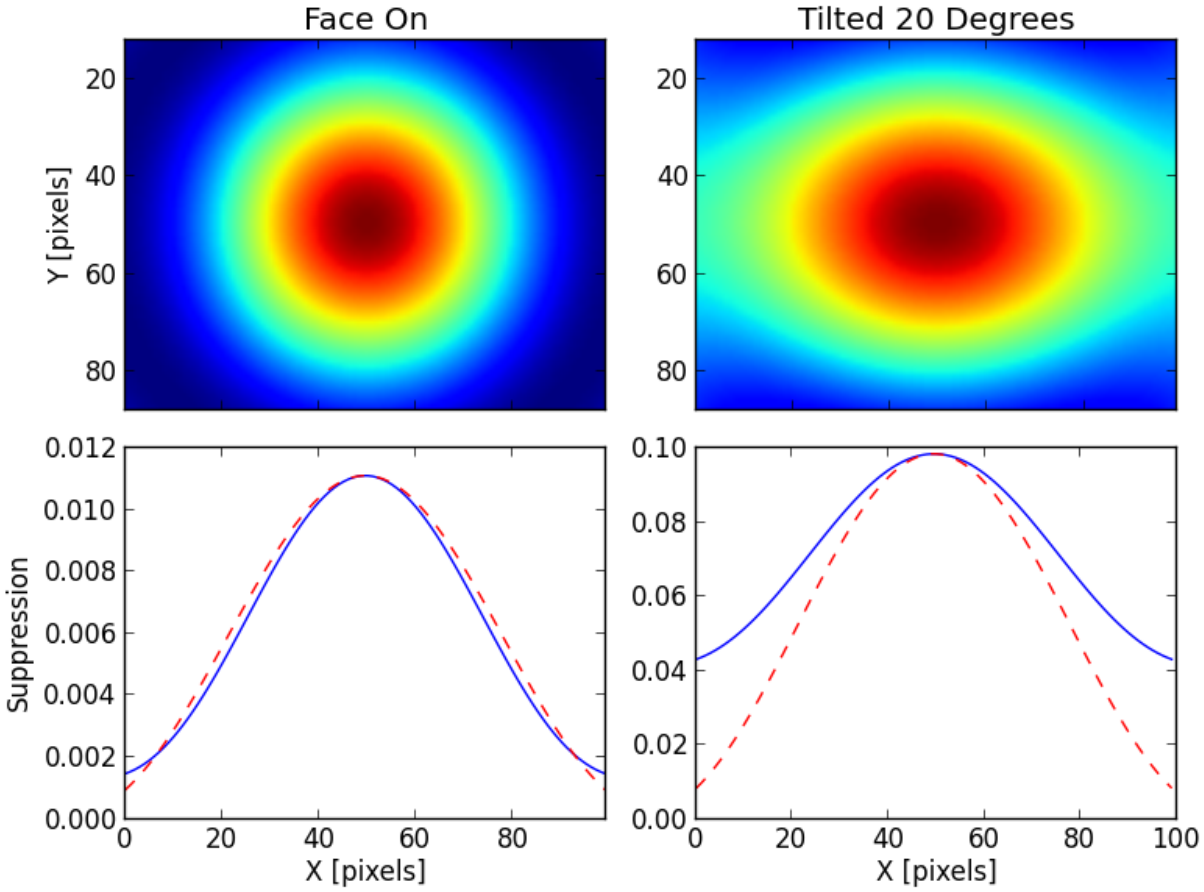

Figure 7: The **top** panel shows simulated pupil images using TDEM13 parameters of Table 1. In the **bottom** panel, the **blue** line is a cross-section of the image and the **red** dashed line is a model fit to the image using Equation 3. The **left** panel is when the starshade is face-on, the **right** panel is after the starshade has been tilted by 20°.

unblocked images will be taken in the shortest possible timeframe in order to sample the same atmospheric conditions. A number of filters from 1 μm - 2 μm will be used to assess the wavelength response of the starshade. Other standard image processing, such as dark subtractions, will also be done. Our main measurements to compare to the models will be the peak value and width of the central spot of the diffraction pattern.

The analysis for Milestone 2 will be to extract the relative position of the starshade from the images and compare against the known movement of the starshade. The relation between movement of the starshade and the position extracted from the images will be compared against theoretical predictions. We will investigate different methods of extracting the position from the images (centroiding, model fitting, etc.), which will be an additional informative product of this study.

The Final Report to be submitted to the Exoplanet Exploration Program will contain the following data products:

1. Model predictions of the resultant diffraction pattern incident on the pupil in units of suppression.
2. Pupil plane images normalized by unblocked source.
3. Agreement between measurements and predictions for the diffraction pattern at long wavelengths.
4. Model predictions of relative position measurements of the starshade calculated from simulated images.
5. Relative position measurements of the starshade calculated from pupil images.
6. Agreement between measurements and predictions for relative position sensing.
7. Quantification of atmospheric turbulence seen during testing.

6. Success Criteria

For each milestone we list the criteria that serve as necessary requirements for the successful completion of that milestone along with the rationale for why the criteria demonstrate the intent of the milestone.

6.1. Milestone #1

With the starshade placed directly in the line of sight to a NIR source, measure the diffraction pattern in the starshade shadow and compare against numerical models to assess model validity.

The purpose for this first milestone is to demonstrate that at $\lambda > 1.5$ μm we can recover enough flux for a guiding signal at an adequate signal-to-noise. A perfectly circular disk should recover 100% of the intensity, however at these wavelengths, the apodization of the starshade's petals is still working to extinguish some of the light. Theory predicts the on-axis intensity in the shadow of a starshade at $\lambda = 2$ μm to be 1% of the unblocked source intensity, but as this is unexplored territory, we cannot say for certain what level of light will be recovered. Our success criteria is to measure the level of diffracted light at different wavelengths (1 μm - 2 μm) and demonstrate agreement with numerical models to 10%. These results will allow us to evaluate if the recovered flux is significantly bright and robust to be used as a guiding signal.

As mentioned in Section 4.3, we must rely on optical models to predict the flight performance of a starshade. Comparing images taken in the field with those predicted by our models will be an important anchor for model validation at long wavelengths. Additionally, working at a longer wavelength will allow us to work at a flight-like Fresnel number, an important

consideration when validating the models. The measurement we are interested in for use as a formation flying signal, is the shape of the diffraction pattern in the shadow of the starshade. Comparison of the relative intensity and width of the central peak in the diffraction pattern will allow us to assess the validity of our models at these wavelengths. Our success criteria for this milestone is to obtain measurements at these wavelengths and document the agreement between experimental results and models. Our goal is for the agreement between results and models to be below 10%.

6.2. Milestone #2

Measure relative position of starshade and telescope and compare to known position to within error imposed by atmospheric seeing.

The purpose of Milestone 2 is to demonstrate we can use the light diffracted around the starshade to provide high-precision position measurements. The accuracy of these measurements depend on signal-to-noise, telescope resolution, and size of the central diffraction peak relative to the aperture size. Performing these tests in the atmosphere will also limit accuracy, but movements that are larger than the expected error due to seeing should provide a clear signal. Our success criteria are to define a relation between the movement of the starshade and the movement of the spot of Arago in the pupil plane and compare this relation to predictions. Our accuracy will be limited by the error introduced by atmospheric seeing. The accuracy of position sensing required by the NWO mission is 2% the width of the spot of Arago ($\pm$10 cm with a 5 m diameter spot). In order to reach that level with these tests, we need an accuracy of 240 μm, or $\sim$1 pixel. By monitoring off-axis lights at the distance of the starshade, we can estimate the contribution of image wander due to the atmosphere. Our goal for this milestone is for the RMS fluctuations detected in the position of the starshade as detected by the spot of Arago to agree with the RMS fluctuations seen in the positions of the off-axis lights by 10%. These data will allow us to assess the *Arago Sensor* as a means for accurate, long-range position sensing.

7. Schedule

The schedule for the proposed work is outlined in Figure 8. We have allotted 2 trips, each lasting 1-week, to conduct tests in the field. Each trip, and the subsequent data analysis, will help assess the system design and will allow us to iterate on the design needed to reach our TDEM milestones. Hardware will be assembled, calibrated, and tested at CU before moving to the field. Data will be analyzed after each test to assess the success criteria, any unforeseen issues that arose, and progress made toward the TDEM milestone. Since this is technology development, problems will most certainly arise, but we are confident in our ability to address them and adapt accordingly.

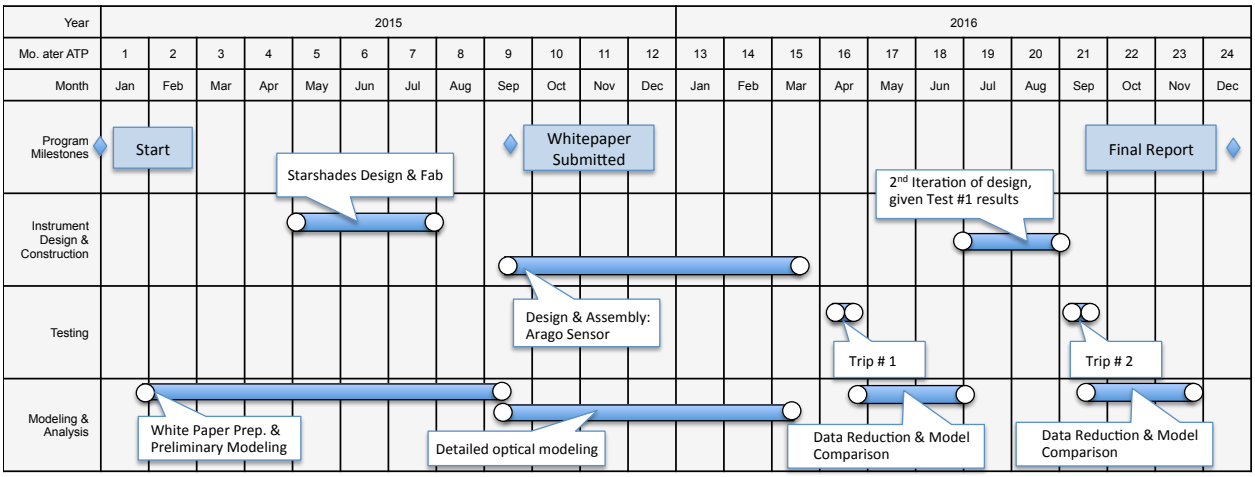

Figure 8: Schedule of work

The general work schedule is detailed below:

- Jan 2015: Project Start
- Jan – Sep 2015: Complete whitepaper report and do preliminary models of the spot of Arago. The whitepaper will outline the success criteria of the technology we propose to develop. Preliminary models will help inform milestone development
- May – Jul 2015: Design starshades and send out for fabrication
- Sep 2015: Whitepaper submitted
- Sep 2015 – Mar 2016: Design and assemble the optics of the Arago sensors, starshade mounting stages, and light sources. Includes calibration of optics at CU.
- Apr 2016: Trip #1.
- Apr – Jul 2016: Analysis of trip #1 data and model comparisons.
- Jul – Sep 2016: Iteration of optics design given results from trip #1.
- Sep 2016: Trip # 2.
- Sep – Dec 2016: Analysis of trip #2 data and model comparisons.
- Dec 2016: Final Report submitted

References

Cash, W. 2006, Nature, 442, 51

Cash, W., Kendrick, S., Noecker, C., et al. 2009, Proc. Soc. Photo-Opt. Instrum. Eng., 7436, 743606

Cash, W. 2011, ApJ, 738, 76

Charnotskii, M. 2011, Proc. Soc. Photo-Opt. Instrum. Eng., 8161, 816103

Fried, D. L. 1966, Journal of the Optical Society of America (1917-1983), 56, 1372

Glassman, T., Casement, S., Warwick, S., & Novicki, M. 2014, Proc. Soc. Photo-Opt. Instrum. Eng., 9143, 91432O

Glassman, T. M., Warwick, S., Novicki, M., & Smith, D. 2015, American Astronomical Society Meeting Abstracts, 225, #338.24

Noecker, M. C. 2007, Proc. Soc. Photo-Opt. Instrum. Eng., 6693, 669306

Noecker, M. C. 2010, Journal of Guidance, Control, and Dynamics, 137, 10-39

Novicki, M., Warwick, S., Smith, D., et al. 2016, American Astronomical Society Meeting Abstracts, 227, submitted

Sommargren, G. E., & Weaver, H. J. 1990, Appl. Opt., 29, 4646-4657

Warwick, S., Glassman, T., Novicki, M., et al. 2014, ExoPAG # 10, Boston, MA